LIP-STUDENTS-25-31

Measuring thin films thickness using surface plasmon resonance

Rafael Alves[1,a]

[1] *Lisbon School of Engineering (ISEL), Lisbon, Portugal*
[2] *Laboratório de Instrumentação e Física Experimental de Partículas, Lisbon, Portugal*
[3] *Faculdade de Ciências da Universidade de Lisboa, Portugal*

Project supervisor: João Gentil[2], José Figueiredo[2,3]

December 4, 2025

Abstract. Surface Plasmon Resonance (SPR) is a highly sensitive optical technique for characterizing thin metallic films and probing variations in refractive index at metal–dielectric interfaces. This work presents an experimental investigation of SPR phenomena using the Kretschmann configuration with gold thin films of varying thickness deposited on glass substrates. Two complementary experimental approaches were implemented: a laser-based setup using a HeNe laser (638.2 nm) with visual detection, and a broadband setup employing a white LED source coupled to a mini-spectrometer. Qualitative evidence of surface plasmon excitation was obtained through direct observation of intensity modulation in reflected laser beams as a function of incident angle. However, quantitative measurements were hindered by several experimental limitations, including uncertain film thickness, poor film adhesion to glass substrates, and insufficient signal-to-noise ratio in spectroscopic measurements. A systematic analysis of these limitations is presented, including control experiments to assess optical contact quality using index-matching oil. Despite the limited quantitative results, this work demonstrates the fundamental principles of SPR and provides valuable insights into the experimental challenges associated with thin film plasmonics, particularly regarding sample preparation, optical alignment, and detection methods.

Keywords: Plasmonics, SPR, Thin Films

1 Introduction

Thin metallic films are at the core of numerous optical and electronic applications, where their structural and optical properties determine the overall device performance. Understanding and characterizing these properties at the nanoscale is therefore of great relevance in both fundamental and applied research. Among the available optical techniques, **Surface Plasmon Resonance (SPR)** has proven to be one of the most sensitive approaches for probing variations in refractive index and film thickness, offering non-destructive and real-time measurement capabilities.

SPR arises from the resonant coupling between incident light and the collective oscillations of conduction electrons at a metal–dielectric interface. The resulting resonance condition depends strongly on the dielectric environment and on the geometry of the metallic layer, allowing minute changes in optical or structural parameters to be detected. Owing to these features, SPR has become a versatile tool across different scientific domains, ranging from material characterization to biosensing and nanophotonics.

In this work, the fundamental principles of surface plasmon resonance are explored, together with its implementation for the optical study of thin metallic films. The aim is to provide a physical understanding of the phenomenon and to illustrate how plasmonic effects can be exploited to determine film properties at the nanometric scale.

The following section introduces the basic physical principles of Surface Plasmon Resonance (SPR).

[a] e-mail: rafael.mdoalves@gmail.com

1.1 Surface Plasmon Resonance (SPR)

The SPR is an optical phenomenon that occurs when plane-polarized light interacts with a thin metallic film under total internal reflection conditions, and is used in biological and biomedical fields to study biomolecular interactions by observing the change of the refracted light coming from a prism [1].

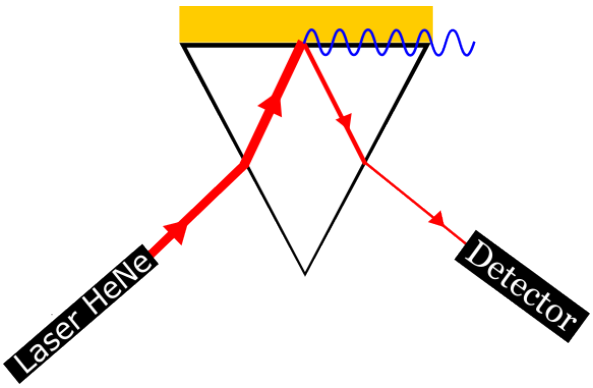

Figure 1. The Kretschmann configuration diagram.

Throughout this paper, this concept will be explained to provide a clearer understanding of the previous statement.

A plasmon can be understood as the quantum associated with the collective oscillation of free electrons in a plasma, or in this case, in thin metal films. At first glance, this concept may appear highly abstract, yet it underlies phenomena we encounter daily. The characteristic metallic luster of bulk metals originates from the

collective oscillations of conduction electrons, known as surface plasmons[1]. When an electromagnetic wave impinges on the metal, its oscillating electric field drives the conduction electrons to collectively oscillate against the fixed ionic lattice, as illustrated in Figure 2. This collective motion is governed by the material's *plasma frequency* (ω_p), which represents the natural oscillation frequency of the free electron gas. For incident light with frequency $\omega < \omega_p$, the electrons efficiently screen the external field, leading to a negative real part of the dielectric function. As a consequence, the oscillating electrons re-radiate an electromagnetic wave that is phase-shifted by π relative to the incident field—resulting in strong reflection, the fundamental origin of metallic luster.

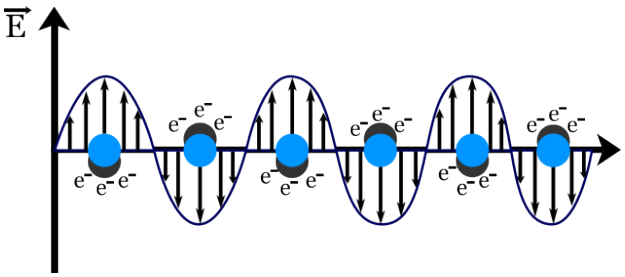

Figure 2. Electrons' oscillation given by an electric field.

Before proceeding, it is important to clarify the distinction between bulk (3D) metals and thin metallic films. In bulk materials, the conduction electrons occupy a continuous band, and the plasmon resonance corresponds to bulk plasmons, typically found in the ultraviolet range. However, when the metal thickness is reduced to a few tens of nanometers, comparable to the skin depth of the electromagnetic field (∼ 10–30 nm), the translational symmetry in the z-direction is broken and the k_z component becomes quantized. This leads to the emergence of surface plasmon modes with a quasi-two-dimensional (2D-like) character [2–4].

For a single metal–dielectric interface, the dispersion relation of the surface plasmon polariton (SPP) is given by

$$k_x = \frac{\omega}{c}\sqrt{\frac{\varepsilon_m(\omega)\,\varepsilon_d}{\varepsilon_m(\omega)+\varepsilon_d}}, \tag{1}$$

where $\varepsilon_m(\omega)$ is the dielectric function of the metal and ε_d the permittivity of the dielectric medium.

In contrast, for a thin metallic film of thickness d, the coupling between the fields at the two interfaces leads to symmetric and antisymmetric modes. The dispersion relations are obtained from the boundary conditions and read [4]:

$$\tanh\left(\frac{k_m d}{2}\right) = -\frac{\varepsilon_m k_d}{\varepsilon_d k_m} \quad \text{(symmetric mode)}, \tag{2}$$

$$\coth\left(\frac{k_m d}{2}\right) = -\frac{\varepsilon_m k_d}{\varepsilon_d k_m} \quad \text{(antisymmetric mode)}, \tag{3}$$

with $k_m = \sqrt{k_x^2 - \varepsilon_m(\omega)(\omega/c)^2}$ and $k_d = \sqrt{k_x^2 - \varepsilon_d(\omega/c)^2}$. These expressions show explicitly how the film thickness alters the plasmonic response compared to the bulk case.

1.2 Surface Plasmon Resonance Configurations

Surface Plasmon Resonance (SPR) exploits the resonant excitation of surface plasmons—collective oscillations of conduction electrons at a metal–dielectric interface—by an incident electromagnetic wave. The excitation condition requires matching the in-plane momentum of the photons with that of the surface plasmons [5]. Because light in air or a dielectric alone lacks sufficient tangential momentum, prism-based coupling schemes are used to achieve this phase-matching condition. The two most common coupling geometries are the Kretschmann and Otto configurations [6, 7].

In the **Kretschmann configuration**, a thin metallic film (typically gold or silver) is deposited directly onto one face of a high-refractive-index prism. Light is incident through the prism at an angle above the critical angle, undergoing total internal reflection at the metal–dielectric interface. The resulting evanescent field penetrates through the thin metal layer and can excite surface plasmons at the outer metal–dielectric boundary. This configuration is the most widely used due to its mechanical robustness and ease of optical alignment [8].

In the **Otto configuration**, the metallic layer is separated from the prism by a thin dielectric gap (such as air or another low-index medium). Light undergoes total internal reflection at the prism–dielectric interface, and the evanescent field extending across the gap can couple to the surface plasmons at the metal surface [6]. Although this geometry provides greater control over the coupling distance, it is experimentally more demanding since the nanometric air gap must be precisely maintained [9].

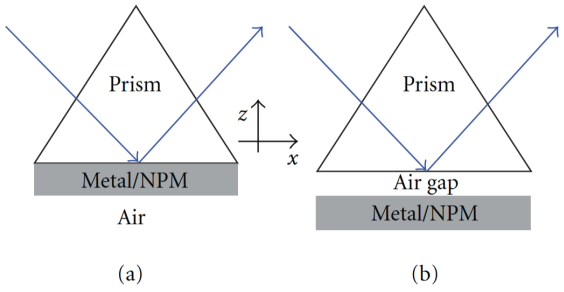

Figure 3. Kretschmann configuration (left), Otto configuration (right).[10]

1.3 Thin Films for SPR

The performance of surface plasmon resonance systems is fundamentally determined by the metallic thin film proper-

[1] The term "surface" is used because the plasmon resonance is localized within approximately 100 nm from the surface.

ties. Film thickness, material composition, surface roughness, and deposition method critically influence the resonance characteristics and sensor sensitivity [11].

Material Selection and Thickness

Gold is the preferred material for SPR applications due to its chemical stability, oxidation resistance, and favorable optical properties in the visible and near-infrared range [8]. Silver films yield sharper resonance curves due to lower damping losses, but their oxidation susceptibility limits biological applications [5]. The optimal thickness for gold films ranges between 40 and 60 nm. Thinner films produce weak, poorly defined resonance peaks, while thicker films exhibit excessive damping that broadens the resonance curve and reduces angular sensitivity [7].

Deposition Techniques

Two primary deposition methods were employed in this work: magnetron sputtering and thermal evaporation. Magnetron sputtering typically yields denser, more uniform films with finer grain structure and superior adhesion, making it preferable for high-sensitivity measurements [12]. Three gold films of varying thickness were prepared by direct sputtering onto glass substrates.

Thermal evaporation was used for one additional sample, employing a distinct preparation procedure. In this technique, the metal is heated until it vaporizes and condenses onto a release substrate. The resulting free-standing film is then transferred to the glass slide through a "fishing" process, where the film is floated off and picked up by the target substrate [13]. This transfer method can introduce additional surface irregularities and potential film discontinuities compared to direct deposition, which may affect the SPR characteristics [14].

Adhesion Layers and Substrate Configuration

Direct gold deposition on glass exhibits poor adhesion. An ultrathin adhesion layer (1–3 nm) of chromium or titanium is commonly used for sputtered films [11]. While essential for mechanical stability, these layers introduce optical damping that slightly degrades resonance sharpness. In our experimental setup, the thin films on glass slides, rather than directly on the prism, offered practical advantages for sample handling and interchangeability between different film thicknesses during measurements.

2 Experimental Setups

Given the configurations aforementioned, the Kretschmann configuration was chosen on account of its simplicity when compared to Otto's, which requires maintaining an air gap of only a few nanometers and therefore implies a meticulous assembly.

This section describes the optical setups and instrumentation used throughout the experiments. The setups were designed to excite and detect Surface Plasmon Resonance (SPR) phenomena using both monochromatic and broadband light sources. A schematic overview of the main optical elements, their labels, and functions is summarized in Table 1. This nomenclature is consistent with the one used in the figures of this section.

Four thin gold films were employed in the experiments, which can be seen in Figure 4. The three slides placed in the case were sputtered and are sorted in increasing thickness from left to right, whereas the gold sample in the bottom-left corner was deposited by thermal evaporation.

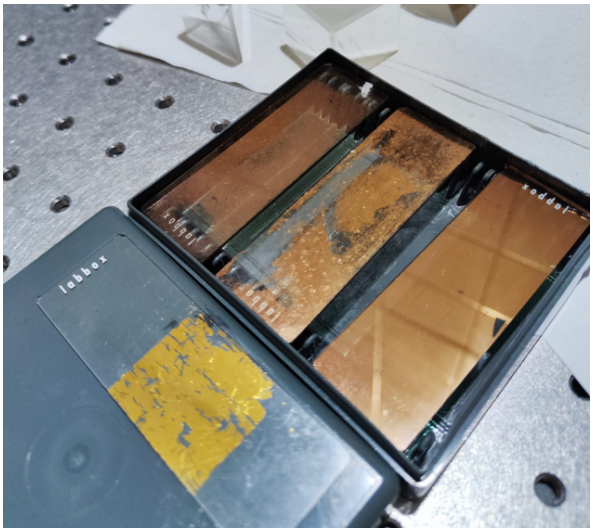

Figure 4. Picture of the gold samples. The three slides on the slide case were sputtered and are sorted in increasing thickness from left to right. The gold sample in the bottom-left corner was deposited by the thermal evaporator.

A significant experimental constraint is the absence of direct thickness measurements for each sample; therefore, the resulting data may be influenced by variations in the film thickness.

The following sections are organized according to the source of electromagnetic radiation used: first, the laser-based setups are described (Section 2.1), followed by the broadband light configuration (Section 2.2).

2.1 Laser Setups

For the laser setups, a HeNe laser with a wavelength of 638.2 nm and a Thorlabs PL201 laser with a typical wavelength of 520 nm were used. However, most of the study focused on the HeNe laser due to its resonance with gold. This choice is supported by the fact that the damping of the Surface Plasmon Resonance (SPR) is minimized when using red light ($\lambda \approx 633$ nm), as this wavelength lies far from the strong coupling with gold's interband transitions. The interband transition absorption of gold occurs at around 2.65 eV (approximately 468 nm). Since 520 nm (green light) is closer to this strong absorption region than 638.2 nm, the HeNe laser provides a **sharper and less damped** resonance curve [15].

During the development of the laser-based setup, several optical configurations were tested to optimize the surface plasmon excitation and detection. Although not represented in the schematic diagrams (Figures 5 and 6), initial attempts were made using simplified arrangements—such as directing the laser beam through one or

Table 1. Optical components used in the experimental setups and their corresponding nomenclature.

Label	Component Description
L	Biconvex lens (Thorlabs)
P	Linear polarizer (Glan–Thompson type, Thorlabs)
Ph	Pin hole aperture (adjustable diameter, Thorlabs)
OL	Objective lens (20×, NA = 0.40)
PR	Right-angle BK7 prism (n = 1.515, Thorlabs)
GON	Goniometer (PASCO Optics Bench UNSET, angular precision ≈ 0.1°)
BS	Beam splitter (50:50, non-polarizing, Thorlabs)
M	Kinematic mirror mounts KM100-E01 with UV–Vis dielectric mirrors (Thorlabs)
S	Sample holder with interchangeable thin-film slides

two polarizers before reaching the prism, or removing intermediate optical elements like the mirror or spatial filtering system. However, a critical limitation was encountered with multiple polarizers: each polarizer reduces the transmitted intensity by approximately 50%, meaning that a configuration with two polarizers would retain only 25% of the initial beam intensity. This significant loss made it difficult to observe clear resonance features, particularly when relying on visual detection. It should be noted that these preliminary measurements did not employ any spectrometer or camera for quantitative data acquisition. Instead, detection was performed by direct visual observation of the reflected beam intensity at different angles—an approach inspired by educational demonstration videos [16, 17]. While this method allowed for qualitative identification of the resonance angle, it inherently limited the precision and reproducibility of the measurements.

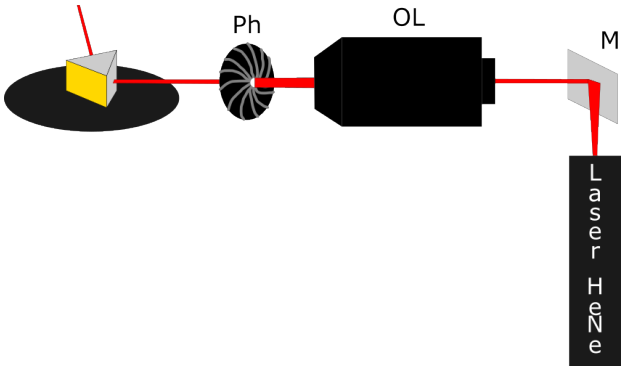

Figure 5. Laser-based setup for surface plasmon resonance excitation using a HeNe laser (λ = 638.2 nm). The beam is directed by a mirror (M) and focused by an objective lens (OL) onto a pinhole (Ph), forming a spatial filtering system that removes higher-order modes and beam imperfections. The transmitted beam is then collimated and directed toward the prism, providing a clean and uniform illumination spot for improved angular sensitivity in SPR measurements.

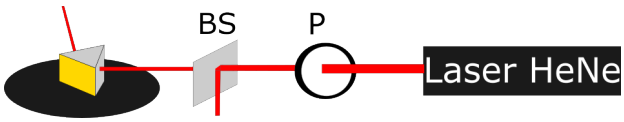

Figure 6. Experimental configuration using a HeNe laser and a non-polarizing beam splitter (BS). The BS was initially expected to act as a polarizing element to separate s and p components; however, since it transmits and reflects both polarizations equally, a linear polarizer (P) was added to ensure p-polarized light—necessary for surface plasmon excitation at the metal–dielectric interface.

2.2 Light Setup

For the broadband measurements, a white LED lamp was used as the light source. Although not designed for laboratory spectroscopy, its broad visible emission spectrum was suitable for the reflectivity measurements required in this experiment. The emitted light was collimated using a biconvex lens (L) and directed towards the prism in the Kretschmann configuration. The reflected light was collected by an optical fiber (OpF) and transmitted to a Hamamatsu mini-spectrometer for spectral analysis.

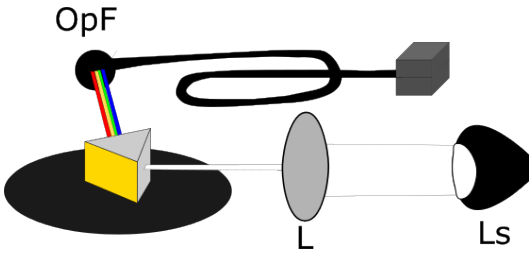

Figure 7. Schematic of the broadband light setup. The light source (Ls) emits a white beam that is collimated by a biconvex lens (L) before reaching the prism. The reflected light is collected by an optical fiber (OpF) connected to a Hamamatsu mini-spectrometer, where the reflected intensity is analyzed as a function of the incidence angle.

To improve the mechanical stability and repeatability of the setup, two custom 3D-printed components were designed and manufactured. The first was an optical fiber holder, compatible with the M6 threaded holes of the optical bench, which ensured precise and rigid positioning of the fiber tip. The second component was a linear

guide that aligned the fiber along the rotational axis of the prism–goniometer assembly, maintaining a constant distance during angular scans. These simple additions greatly improved the reproducibility of the optical alignment.

Photographs of both components are shown in Figure 8 and 9.

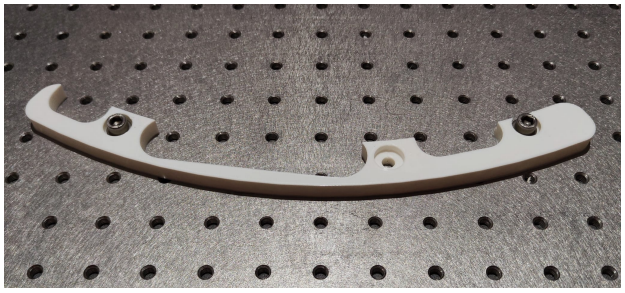

Figure 8. 3D printed barrier/guiding-barrier to the optical fiber holder.

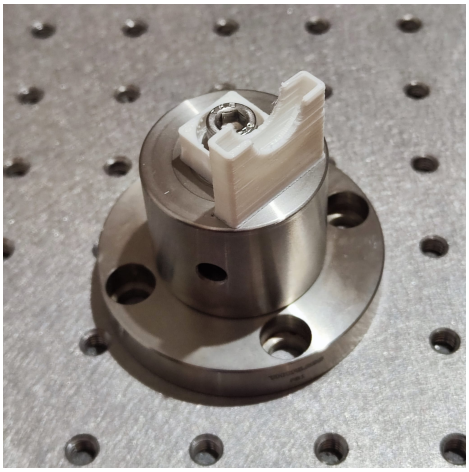

Figure 9. 3D printed adapter to the optical fiber end.

Figure 10. Image showing the 3D parts assembly.

3 Results and Discussion

3.1 Laser-based measurements

Visual observation of the reflected beams revealed qualitative evidence of surface plasmon excitation. As the incident angle was varied using the goniometer, two reflected beams were observed emerging from the prism—a primary beam with higher intensity and a secondary beam with lower intensity. Notably, the secondary beam showed a clear variation in intensity with angle, including instances when it became barely visible or disappeared entirely.

Figure 11 shows selected frames extracted from video recordings during angular scanning. The observed intensity minimum in the secondary beam is consistent with the expected behavior at plasmon resonance, where the incident light couples efficiently into surface plasmon modes at the gold–dielectric interface, resulting in reduced reflection. The fact that the phenomenon was more clearly observable in the weaker secondary beam can be attributed to the reduced saturation effects compared to the primary reflected beam, which remained at high intensity throughout the angular range.

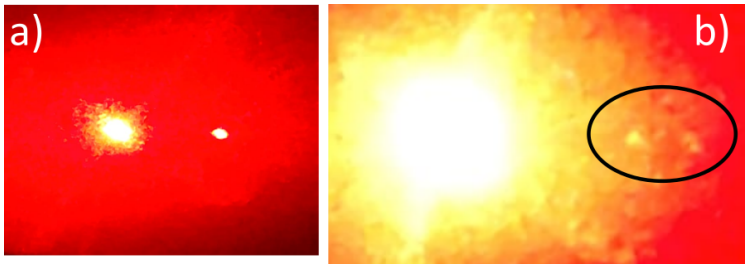

Figure 11. Selected frames extracted from the video recording showing the secondary reflected beam at different incidence angles. (a) Before resonance: the secondary beam is clearly visible. (b) At the resonance angle, the secondary beam intensity drops sharply and momentarily disappears, confirming efficient coupling of the incident light into surface plasmon modes. The reappearance of the beam at larger and smaller angles reinforces the identification of a well-defined resonance condition.

While these observations confirm the occurrence of surface plasmon resonance, the absence of quantitative intensity measurements prevented precise determination of the resonance angle and resonance curve width. The reliance on naked-eye detection, though sufficient for qualitative demonstration, inherently limits the accuracy and reproducibility of angular positioning at the resonance condition.

3.2 Broadband light measurements

Measurements using the white LED source and mini-spectrometer were intended to provide wavelength-dependent reflectivity data as a function of incident angle. However, the recorded spectra showed no significant variation between direct illumination and reflection from the prism–film assembly, regardless of the incident angle.

Figure 12 presents the measured emission spectrum of the white LED source. The broad spectral distribution spans the visible range, which should in principle enable observation of angular-dependent resonance features at different wavelengths. The absence of observable SPR features in the reflected spectra suggests several possible experimental limitations.

3.3 Discussion of experimental limitations

Several factors may have contributed to the limited quantitative results obtained in this work:

Film thickness uncertainty. The absence of independent thickness measurements for each gold film represents a critical limitation. The optimal thickness range for SPR in the Kretschmann configuration is typically 40–60 nm for gold at visible wavelengths [11]. Films outside this range exhibit either weak coupling (too thin) or excessive damping (too thick), both resulting in poorly defined or undetectable resonance features.

Film quality and adhesion. The thermally evaporated film, transferred via the "fishing" technique, likely suffered from surface irregularities, potential discontinuities, and possible contamination during the transfer process. These defects increase scattering losses and broaden the resonance curve.

More critically, the sputtered films exhibited poor adhesion to the glass substrates. During an accidental cleaning of the gold-coated surface with acetone, a portion of the film was easily removed from one of the samples, as visible in Figure 4. This mechanical fragility suggests inadequate bonding between the gold and glass, possibly due to surface contamination during deposition or insufficient substrate preparation. The poor mechanical stability of these films raises concerns about their structural uniformity and optical quality, including the presence of voids, grain boundaries, or weakly bonded regions that could significantly degrade the surface plasmon propagation length and resonance sharpness.

Optical contact at the prism interface. In the configuration used, the gold films deposited on glass slides were placed against the prism face rather than being directly deposited on it. To verify whether poor optical contact could be responsible for the lack of clear SPR features, a control experiment was performed using two prisms with index-matching oil between them. As shown in Figure 13, the laser beam transmitted through this assembly without visible reflection at the interface, confirming that proper optical contact was achieved with the oil. This control test demonstrates that optical contact issues at the prism–film interface are unlikely to be the primary cause of the experimental difficulties, since similar oil-mediated contact was employed during SPR measurements. Nevertheless, the quality of contact between the thin film and the prism may still vary depending on film surface flatness and cleanliness.

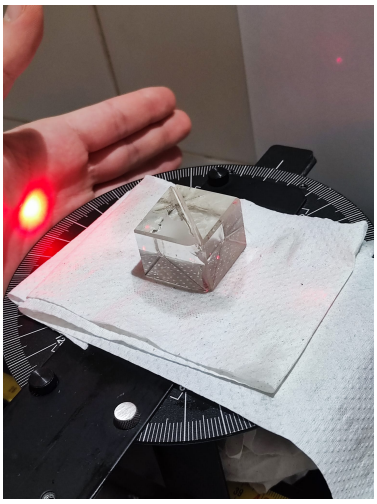

Figure 13. Control experiment showing two prisms with index-matching oil between them. The laser beam passes through without visible reflection at the interface, demonstrating effective optical contact achieved by the oil.

Light source characteristics. The white LED, while convenient and broadband, has significantly lower spectral radiance compared to laser sources. Combined with the losses in the optical path and the reduced collection efficiency of the fiber-coupled spectrometer, the signal-to-noise ratio may have been insufficient to resolve the relatively subtle intensity variations associated with SPR at different angles.

Polarization control. Although a linear polarizer was included in the laser setup, ensuring pure p-polarization is essential for efficient SPR excitation. Any residual s-polarized component does not couple to surface plasmons and contributes only to background reflection. For the broadband measurements, polarization control was not implemented, which further reduces the visibility of resonance features.

Despite these limitations, the qualitative observation of intensity modulation in the laser-based measurements demonstrates that surface plasmon excitation was achieved, at least partially, validating the basic experimental approach and the Kretschmann configuration implementation.

Acknowledgements

I would like to express my sincere gratitude to my supervisors, Researcher João Gentil and Professor José Figueiredo, for their guidance, support, and patience throughout this project. Their expertise and encouragement were invaluable in navigating the experimental challenges encountered during this work.

I am grateful to the NUC-RIA group at LIP for kindly providing one of the gold film samples produced by thermal evaporation, which was essential for comparing different deposition techniques. Special thanks are also due to Mr. Telmo Nunes, responsible for the SEM facility at FCUL, for preparing the three sputtered gold samples used in this study.

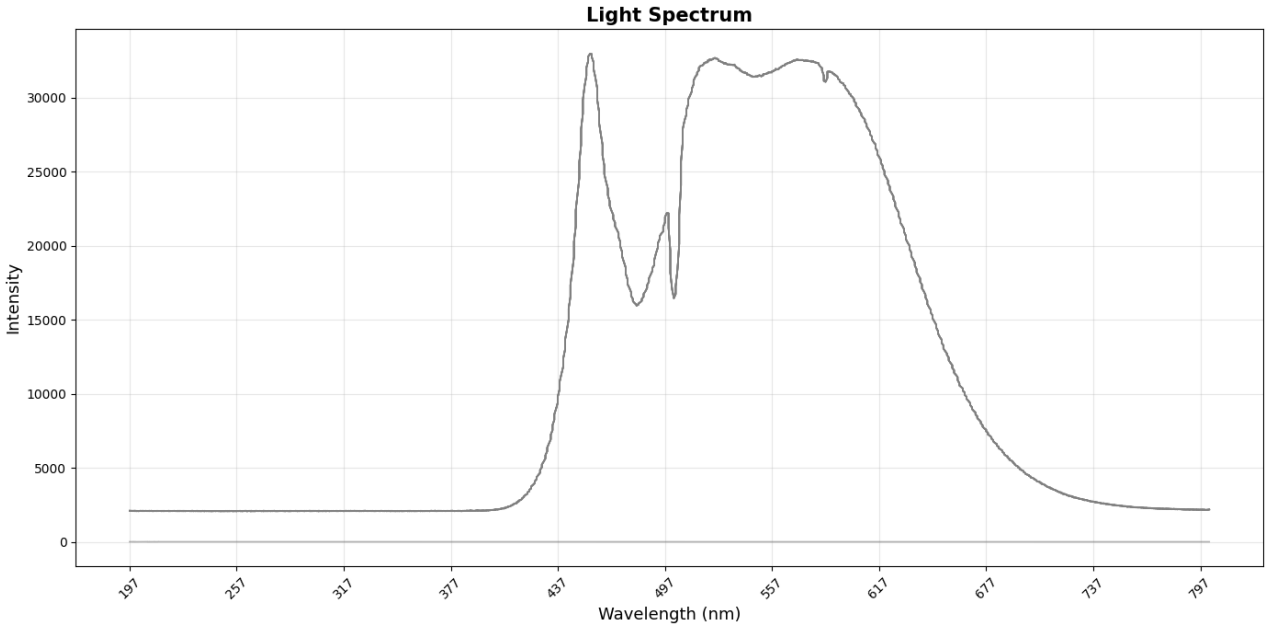

Figure 12. Emission spectrum of the white LED source used in broadband measurements, showing characteristic broad visible emission.

This summer internship provided me with a valuable opportunity to develop my experimental skills in optics and to gain hands-on experience with plasmonic phenomena and thin film characterization techniques. The challenges faced during this work have been as instructive as the successes, reinforcing the importance of careful experimental design and systematic troubleshooting in research.

References

[1] R.V. Stahelin, Molecular Biology of the Cell **24**, 883 (2013)

[2] H. Raether, Surface Plasmons on Smooth and Rough Surfaces and on Gratings, Vol. 111 of Springer Tracts in Modern Physics (Springer, 1988)

[3] S.A. Maier, Plasmonics: Fundamentals and Applications (Springer, 2007)

[4] P. Berini, Physical Review B **61**, 10484 (2000)

[5] H. Raether, Surface Plasmons on Smooth and Rough Surfaces and on Gratings (Springer, Berlin, 1988)

[6] A. Otto, Zeitschrift für Physik **216**, 398 (1968)

[7] E. Kretschmann, H. Raether, Zeitschrift für Naturforschung A **23**, 2135 (1968)

[8] J. Homola, S. Yee, G. Gauglitz, Sensors and Actuators B: Chemical **54**, 3 (1999)

[9] A.V. Zayats, I.I. Smolyaninov, A.A. Maradudin, Physics Reports **408**, 131 (2005)

[10] A. Estroff, B. Smith, International Journal of Optics **2012** (2012)

[11] J. Homola, Surface Plasmon Resonance Based Sensors (Springer, Berlin, 2006)

[12] P.B. Johnson, R.W. Christy, Physical Review B **6**, 4370 (1972)

[13] S. Zhu, D.P. Langley, D. Gu, Y. Tian, Applied Physics Letters **102**, 161909 (2013)

[14] Y. Jiang, H.Q. Wang, H. Wang, B.R. Gao, Y.W. Hao, Optics Communications **260**, 433 (2006)

[15] O. Pluchery, R. Vayron, K.M. Van, European Journal of Physics **32**, 585 (2011)

[16] engineerguy, Surface plasmon resonance (2012), `https://www.youtube.com/watch?v=RO6Rq6-cqsY`

[17] Nanooptics Group, Surface plasmon resonance demonstration (2015), `https://www.youtube.com/watch?v=KDKJVzwkNos`